NUMERICAL STUDY OF BOILING AND NATURAL CONVECTION IN CAPILLARY POROUS MEDIA USING THE TWO-PHASE MIXTURE MODEL

C. Y. Wang, C. Beckermann, and C. Fan
Department of Mechanical Engineering, University of Iowa, Iowa City,
Iowa 52242, USA

A newly developed two-phase mixture model is applied, in conjunction with a control-volume-based finite difference method, to numerically investigate boiling with thermal convection in a porous layer heated from below. The numerical procedure employs a fixed grid and avoids tracking explicitly the moving interface between the liquid and two-phase regions. Numerical results are obtained to shed light on the intricate interactions between boiling and natural convection as well as to explain experimental observations. Four distinct flow patterns that were observed in previous experiments are predicted. A quantitative comparison of the predicted and measured vapor volume fraction in the porous bed shows good agreement. The numerical results also agree with published linear stability results. In addition, the present study documents the effects of important parameters such as Rayleigh number, bottom heat flux, and aspect ratio.

INTRODUCTION

Liquid/vapor phase change and associated two-phase flow in porous media occur in a wide variety of systems. Examples include geothermal systems, postaccident scenarios of nuclear reactors, heat pipes, drying processes, and latent heat energy storage systems using packed beds.

In spite of the importance of these problems in engineering, their numerical analysis has been severely hindered due to several features inherent to two-phase flow with phase change in porous media. The first difficulty centers on the fact that the traditional mathematical formulation to describe the transport phenomena, namely, the separate flow model [1], involves a large set of strongly nonlinear governing equations in the two-phase zone. Their solution in a multidimensional domain represents a challenging computational task and has been the subject of numerous studies [2]. Usually, by neglecting the capillary force, the number of main variables can be reduced and the governing equations can be considerably simplified. However, such a simplified model loses generality in low-permeability and heterogeneous media, where the capillary force is significant. The second

NOMENCLATURE

A	aspect ratio ($= L_h/L_w$)	α_s	heat capacitance ratio of solid matrix to liquid $[= \rho_s c_s/(\rho_1 c_1)]$
c	specific heat		
$D(s)$	capillary diffusion coefficient, Eq. (23)	α_v	heat capacitance ratio of vapor to liquid $[= \rho_v c_v/(\rho_1 c_1)]$
$f(s)$	hindrance function, Eq. (20)	β	thermal expansion coefficient
g	gravitational acceleration	γ_h	two-phase advection correction coefficient, Eq. (11)
$\mathbf{g}$	gravitational acceleration vector		
h	enthalpy	Γ_h	effective diffusion coefficient, Eq. (13)
h_{fg}	latent heat of liquid/vapor phase change	$\Delta \rho$	density difference ($= \rho_1 - \rho_v$)
H	volumetric enthalpy	ε	porosity or volume fraction
$\mathbf{j}$	diffusive mass flux	θ	dimensionless temperature $[= (T - T_o)/(T_{sat} - T_o)]$
$J(s)$	capillary pressure function		
k_r	relative permeability	λ	relative mobility or latent heat parameter $\{= h_{fg}/[c_1(T_{sat} - T_o)]\}$
k_{eff}	effective thermal conductivity		
K	absolute permeability	μ	viscosity
L	length	ν	kinetic viscosity
Le_c	Lewis number of capillary diffusion, $[= (\varepsilon K)^{1/2} \sigma c_1/(\upsilon_1 k_{eff})]$	$\tilde{\nu}$	ratio of kinetic viscosity ($= \nu_v/\nu_1$)
p	pressure	ρ	density
q_w	bottom heat flux	$\tilde{\rho}$	density ratio ($= \rho_v/\rho_1$)
Q_w	dimensionless bottom heat flux $\{= q_w L_h/[k_{eff}(T_{sat} - T_o)]\}$	σ	surface tension
		ψ	stream function
Ra	Rayleigh number in the liquid region $[= KL_h g \rho_1 \beta_1(T_{sat} - T_o)c_1/(\upsilon_1 k_{eff})]$	Ω	effective heat capacitance ratio, Eq. (12)
$\mathrm{Ra}_{2\phi}$	Rayleigh number in the two-phase region $[= KL_h g \rho_1 c_1/(\upsilon_1 k_{eff})]$	**Subscripts**	
s	liquid saturation		
t	time	c	capillary
T	temperature	h	in vertical direction
$\mathbf{u}$	superficial or Darcian velocity vector	l	liquid phase
		o	top boundary
x	coordinate in horizontal direction	sat	saturated state
X	dimensionless x coordinate	v	vapor phase
y	coordinate in vertical direction	w	in horizontal direction
Y	dimensionless y coordinate	κ	"kinetic" property

obstacle to a numerical simulation of two-phase flow in porous media is associated with the presence of a moving and irregular interface separating the single- and two-phase regions [3, 4]. The location of this phase interface is not known a priori and depends on the coupled flows in both regions. If based on the traditional separate flow model, a numerical procedure for such a multiregion problem needs to explicitly track the moving interface, thus calling for complex coordinate mapping or numerical remeshing [3].

Recognizing that the separate flow model is not well suited for the analysis of two-phase flow in porous media with and without phase change, Wang and Beckermann [5] proposed a two-phase mixture model in which the conservation equations of mass, momentum, and energy are formulated for the two-phase

mixture. The new model has several advantages over the conventional separate flow model. First, significantly fewer governing equations (i.e., only those for the two-phase mixture) are required to be solved. Second, the model is a single-domain formulation in which each of the conservation equations is valid in all regions throughout the problem domain. Hence, there is no need to prescribe complex internal boundary conditions at the phase interface and to track the moving interface explicitly. This offers great simplifications in a numerical implementation of two-phase flow problems. Finally, the two-phase mixture model is mathematically exactly equivalent to the traditional separate flow model, in the sense that no additional approximations are introduced and the two-phase characteristics (i.e., the phase velocities) are readily attainable from the fields of the mixture variables.

Although the above features were discussed in detail in Ref. [5], and the advantages of the new model in the analytical solution of a boundary layer two-phase flow problem were demonstrated in Ref. [6], a general purpose numerical method, which is based on the two-phase mixture model and can be applied to a large class of phase change flow problems in capillary porous media, has not yet been developed. The objective of this paper is therefore to formulate such a numerical methodology in detail. Specifically, we utilize the error vector propagation (EVP) method [7] to solve the pressure equation of the Poisson type, and the control-volume-based finite difference scheme of Patankar [8] for the energy equation. Boiling with natural convection in a horizontal porous cavity heated from below is selected as a computational example. Comprehensive numerical results are presented to highlight the rich physics behind the interacting boiling and natural convection phenomena, to explain previous experimental observations, as well as to demonstrate the utility of the two-phase mixture model in a numerical solution.

MATHEMATICAL FORMULATION

Conservation Equations

As described in a recent paper [5], the liquid/vapor mixture is viewed similar to a binary chemical mixture, with the two flowing phases represented as different species. Then a set of conservation equations of mass, momentum, and energy for such a mixture can be derived. By invoking the Boussinesq approximation, which considers the density variation only in the buoyancy term of the momentum equation in the single-phase region, and assuming that the two-phase region is isothermal at the boiling temperature (T_{sat}), the governing equations can be written as follows [5]:

Continuity

$$\varepsilon \frac{\partial \rho}{\partial t} + \nabla \cdot (\rho \mathbf{u}) = 0 \tag{1}$$

Momentum

$$\mathbf{u} = -\frac{K}{\mu}(\nabla p - \rho_\kappa \mathbf{g}) \tag{2}$$

Energy

$$\Omega \frac{\partial (\rho h)}{\partial t} + \nabla \cdot (\gamma_h \rho \mathbf{u} h) = \nabla \cdot (\Gamma_h \nabla h)$$

$$+ \nabla \cdot [\Gamma_h (h - h_{vsat}) \nabla \ln \rho]$$

$$+ \nabla \cdot \left[f(s) \frac{K \Delta \rho h_{fg}}{\nu_v} \mathbf{g} \right] \qquad (3)$$

where volumetric heat generation is excluded and the mixture properties and variables are defined as follows:

Density

$$\rho = \rho_l s + \rho_v (1 - s) \qquad (4)$$

Kinetic density

$$\rho_\kappa = \rho_l [1 - \beta_l (T - T_o)] \lambda_l(s)$$

$$+ \rho_v [1 - \beta_v (T - T_{sat})] \lambda_v(s) \qquad (5)$$

Viscosity

$$\mu = \frac{\rho_l s + \rho_v (1 - s)}{(k_{rl}/\nu_l) + (k_{rv}/\nu_v)} \qquad (6)$$

Velocity

$$\rho \mathbf{u} = \rho_l \mathbf{u}_l + \rho_v \mathbf{u}_v \qquad (7)$$

Enthalpy

$$\rho h = \rho_l s h_l + \rho_v (1 - s) h_v \qquad (8)$$

In the above equations, a quantity without a subscript is reserved for the mixture, while the subscripts l and v denote liquid and vapor properties, respectively. The other symbols are defined in the nomenclature, and their physical meanings have been provided in Ref. [5].

It is important to recognize that both the mixture enthalpy and velocity are mass averages of their corresponding phase quantities. Moreover, the conservation equations, Eqs. (1)–(3), are valid throughout a physical domain, including both the single- and two-phase regions. It is noteworthy that the energy equation, Eq. (3), represents a unified form of the temperature equation in the liquid region and the liquid saturation equation in the two-phase region (see below).

For computational convenience, the energy equation can be further simplified by writing it in terms of a volumetric enthalpy, which is defined as

$$H = \rho(h - h_{vsat}) \qquad (9)$$

Then the energy equation is recast into the more simple form,

$$\Omega \frac{\partial H}{\partial t} + \nabla \cdot (\gamma_h \mathbf{u} H) = \nabla \cdot \left(\frac{\Gamma_h}{\rho} \nabla H \right)$$

$$+ \nabla \cdot \left(f(s) \frac{K \Delta \rho h_{fg}}{\nu_v} \mathbf{g} \right) \qquad (10)$$

where the coefficient γ_h is redefined (as opposed to that in Eq. (3) and Ref. [5]) as

$$\gamma_h = \left[s + \frac{\rho_v}{\rho_l} (1 - s) \right] \frac{\lambda_l(s)}{s} \qquad (11)$$

The effective heat capacitance ratio Ω and the effective diffusion coefficient Γ_h are given by

$$\Omega = \varepsilon + \rho_s c_s (1 - \varepsilon) \frac{dT}{dH} \qquad (12)$$

$$\frac{\Gamma_h}{\rho} = D + k_{eff} \frac{dT}{dH} \qquad (13)$$

respectively, where dT/dH is the derivative of the temperature with respect to the volumetric enthalpy. Equations (12) and (13) are again valid in both the single- and two-phase regions. The temperature and liquid saturation can be recovered from the volumetric enthalpy via the following relations [5]:

$$T = \frac{H + \rho_l h_{vsat}}{\rho_l c_l} \qquad H \leq - \rho_l h_{fg}$$

$$T = T_{sat} \qquad -\rho_l h_{fg} < H \leq 0 \qquad (14)$$

$$T = T_{sat} + \frac{H}{\rho_v c_v} \qquad 0 < H$$

and

$$s = 1 \qquad H \leq - \rho_l h_{fg}$$

$$s = \frac{H}{-\rho_l h_{fg}} \qquad -\rho_l h_{fg} < H \leq 0 \qquad (15)$$

$$s = 0 \qquad 0 < H$$

From Eq. (14), it is easy to show that

$$\frac{dT}{dH} = \frac{1}{\rho_l c_l} \qquad H \leq -\rho_l h_{fg}$$

$$\frac{dT}{dH} = 0 \qquad -\rho_l h_{fg} < H \leq 0 \qquad (16)$$

$$\frac{dT}{dH} = \frac{1}{\rho_v c_v} \qquad 0 < H$$

Supplementary Relations

To complete a mathematical system for two-phase flow in capillary porous media, certain supplementary relations are necessary. In this study, the relative permeabilities of the phases are simply chosen as linear functions,

$$k_{rl}(s) = s \qquad k_{rv}(s) = 1 - s \qquad (17)$$

which are commonly used in geothermal reservoir simulations. Following the derivations by Wang and Beckermann [5], the relative mobilities are accordingly given by

$$\lambda_l(s) = \frac{s/\nu_l}{(s/\nu_l) + [(1 - s)/\nu_v]} \qquad (18)$$

and

$$\lambda_v(s) = \frac{(1 - s)/\nu_v}{(s/\nu_l) + [(1 - s)/\nu_v]} \qquad (19)$$

Similarly, the hindrance function $f(s)$ is evaluated from

$$f(s) = \frac{s(1 - s)/\nu_l}{(s/\nu_l) + [(1 - s)/\nu_v]} \qquad (20)$$

and the capillary pressure function $p_c(s)$ is represented by the Leverett function, such that

$$p_c(s) = \left[\frac{\varepsilon}{K}\right]^2 \sigma J(s) \qquad (21)$$

where the functional form of $J(s)$ established by Udell [9] is employed, i.e.,

$$J(s) = 1.417(1 - s) - 2.120(1 - s)^2 + 1.263(1 - s)^3 \qquad (22)$$

Finally, the capillary diffusion coefficient $D(s)$ can be expressed as

$$D(s) = \frac{(\varepsilon K)^{1/2} \sigma}{\mu_l} \frac{s(1-s)}{[(\nu_v/\nu_l)s] + (1-s)}$$

$$\times [1.417 - 4.240(1-s) + 3.789(1-s)^2] \tag{23}$$

Apparently, other combinations of the constitutive relations for the relative permeabilities and the capillary pressure function can be employed without difficulty.

Velocities of the Individual Phases

The two-phase mixture model [5] also establishes the relations for calculating the phase velocities from the mixture velocity field. These are

$$\mathbf{j} = \rho_l \mathbf{u}_l - \lambda_l \rho \mathbf{u} \tag{24}$$

$$-\mathbf{j} = \rho_v \mathbf{u}_v - \lambda_v \rho \mathbf{u} \tag{25}$$

with

$$\mathbf{j} = -\rho_l D(s) \nabla s + f(s) \frac{K \Delta \rho}{\nu_v} \mathbf{g} \tag{26}$$

The term $\mathbf{j}$ denotes a mass diffusion flux. Equation (26) implies that the diffusive flux is directly proportional to the liquid saturation gradient and the gravitational acceleration. The former is known as capillary diffusion, while the latter plays a role in diffusion because of the large density difference between the liquid and vapor phases. It should be pointed out that Eq. (26) is directly derived from the separate flow model without introducing any ad hoc assumption. In other words, Eq. (26) is of a purely theoretical nature. However, an analogy exists between Eq. (26) and the empirical Fick's law, which purports, in another respect, that two-phase flow in porous media can be viewed as a multicomponent mixture flow. With the help of Eqs. (24)–(26), the two-phase characteristics are completely retained in the present two-phase mixture formulation because the phase velocities can be immediately calculated from these equations once the mixture velocity is obtained.

Computational Example

As a numerical example, boiling with natural convection inside a horizontal porous cavity heated from below is chosen for detailed study. This selection is based on several considerations. First, the problem is of great importance in technological fields such as geothermal reservoir engineering and safety analysis of nuclear reactors. Second, it is of fundamental interest to explore the rich phenomena occurring in interacting single- and two-phase flows in porous media. Finally, there is a large body of experimental data available for validation of the present numerical results.

Several numerical studies [3, 4, 10, 11] dealing with the subject have appeared. Of particular interest to the present study is the work by Ramesh and Torrance [3, 10]. They presented a linear stability analysis of the onset of convection and boiling in the porous layer in Ref. [10], which can be used to verify some of the present numerical predictions. Another objective is to study the interaction between boiling and natural convection in the supercritical region, that is, at high Rayleigh numbers. The numerical investigation by Ramesh and Torrance [3] based on the separate flow model provides a few results for a relatively coarse 9×15 grid.

The system consists of a two-dimensional rectangular porous cavity of dimensions $L_w \times L_h$, as shown in Figure 1. The porous medium is assumed to be uniform, isotropic, and initially saturated with a liquid. The cavity is heated from below and cooled from above. The impermeable bottom is subject to a uniform heat flux, and the top boundary is permeable and kept at a constant temperature T_o. The two vertical walls are well insulated. When the bottom heat flux exceeds a certain value, boiling occurs first adjacent to the bottom; the thermodynamic structure of the system then consists of a liquid region overlying a two-phase region.

The appropriate initial conditions for the problem are

At $t = 0$:

$$H = H_o = \rho_l(c_l T_o - h_{vsat}) \tag{27}$$

$$p = 0 \tag{28}$$

and the necessary boundary conditions for Eqs. (1), (2), and (10) are

At $y = L_h$ (top surface):

$$H = H_o = \rho_l(c_l T_o - h_{vsat}) \tag{29}$$
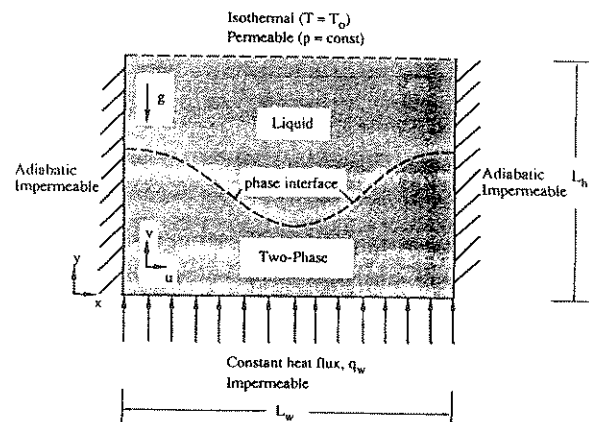
$$p = 0 \tag{30}$$

Figure 1. Schematic of the physical problem and coordinate system.

where Eq. (29) is for isothermal conditions and Eq. (30) is for isobaric conditions. At $y = 0$ (bottom surface):

$$-\frac{\Gamma_h}{\rho}\frac{\partial H}{\partial y} + f(s)\frac{K\Delta\rho h_{fg}}{\nu_v}g = q_w \tag{31}$$

$$\frac{\partial p}{\partial y} = -\rho_\kappa g \tag{32}$$

where Eq. (31) is for a constant heat flux and Eq. (32) is for $v = 0$, impermeable. At $x = 0$ and $x = L_w$ (left and right walls):

$$\frac{\partial H}{\partial x} = 0 \tag{33}$$

$$\frac{\partial p}{dx} = 0 \tag{34}$$

where Eq. (33) is for adiabatic conditions and Eq. (34) is for impermeable conditions.

Difficulties arise when attempting to nondimensionalize the governing equations, Eqs. (1), (2), and (10), and their corresponding initial and boundary conditions, Eqs. (27)–(34). For example, the variable size of the single-phase region and of the flow cross-sectional area preclude the identification of meaningful length and velocity scales. Depending on the selection of these scales, various dimensionless forms may result. Nevertheless, for the purpose of generalization and interpretation, it is useful to present results in a dimensionless form. Omitting details of the nondimensionalization process, it can be shown that the present problem is characterized by 10 dimensionless groups: $\bar{\rho}$, $\bar{\nu}$, α_s, α_v, λ, Le_c, Ra, $Ra_{2\phi}$, Q_w, and A. The first four dimensionless parameters solely depend on the fluid properties, while the remaining groups are the latent heat parameter, the capillary Lewis number, which is the ratio of the capillary diffusion coefficient to the thermal diffusivity, the two Rayleigh numbers, the dimensionless imposed heat flux, and the aspect ratio of the cavity, respectively. The two Rayleigh numbers for the single- and two-phase regions are related by a density ratio, i.e.,

$$\frac{Ra}{Ra_{2\phi}} = \beta_l(T_{sat} - T_o) = \frac{\rho_l \beta_l(T_{sat} - T_o)}{\rho_l} \tag{35}$$

It is clear that the numerator is simply the maximum density variation in the liquid region and the denominator is the density difference between the phases in the two-phase region (since $\rho_l - \rho_v \approx \rho_l$). If the boundary temperature is fixed, the two Rayleigh numbers are not independent.

While these dimensionless parameters permit generalization of the predicted results, caution should be exercised when using them for physical interpretation. The problem lies in the fact that the variation of certain physical (dimensional)

variables would cause variations in more than one dimensionless parameter. One example is the two Rayleigh numbers as shown above. Another example is that the influence of the permeability would be reflected through three dimensionless parameters, namely, Le_c, $Ra_{2\phi}$, and Ra.

In what follows, we numerically solve the set of Eqs. (1), (2), and (10) subject to conditions Eqs. (27)–(34), and report the complete flow, temperature, and liquid saturation fields that prevail in the steady state.

Numerical Method and Validation

Instead of solving the governing equations directly, the momentum equation is substituted into the continuity equation to obtain the following Poisson-type equation:

$$\nabla^2 p = \frac{\nu}{K}\left[\varepsilon\frac{\partial \rho}{\partial t} - \nabla p \cdot \nabla\left(\frac{K}{\nu}\right) + \nabla \cdot \left(\frac{K}{\nu}\rho_k \mathbf{g}\right)\right] \qquad (36)$$

It is convenient to solve this pressure equation and then calculate the flow field via the momentum equation, Eq. (2). In the present paper, Eq. (36) is discretized by the central difference method and solved using the stabilized EVP method developed by Roache [7], which is a direct method for the solution of Poisson equations. The left-hand side of Eq. (36) is intentionally organized to have constant coefficients, in order to maximize the efficiency of the EVP method.

With the knowledge of the pressure field, a modified velocity field can be calculated, which is defined as

$$\mathbf{u}^* = \gamma_h \mathbf{u} = -\frac{K\gamma_h}{\mu}(\nabla p - \rho_\kappa \mathbf{g}) \qquad (37)$$

This modified velocity is directly useful in the energy equation, Eq. (10). The energy equation is solved by the control-volume-based finite difference formulation of Patankar [8]. The combined convective and conductive terms are discretized using the power law scheme [8], and the last term on the right-hand side of Eq. (10) is simply treated as a source term. To obtain an interface diffusion coefficient between two control volumes, the arithmetic mean formula [8] is adopted.

The rectangular domain $L_w \times L_h$ is divided by a uniform and fixed grid consisting of m horizontal and n vertical grid lines. Considerable effort was made to ensure grid size independence of the results presented here. It was found that the results obtained with a 42×42 uniform grid for a square domain are sufficiently accurate and that a finer grid leads to no discernible differences from the results using the 42×42 grid.

The equations are solved as a simultaneous set, and convergence is considered to be reached when the relative errors in the enthalpy and velocity fields between two consecutive iterations are less than 10^{-5}. The total mass and heat flows through the top surface are also calculated and checked against the quantities imposed at the bottom. In all results presented here, mass and energy conservation is ensured to within 0.1% error after convergence is achieved.

To validate the present numerical algorithm, the predictions are compared with available numerical and analytical results. One case is concerned with single-phase natural convection in a horizontal porous cavity with a permeable top boundary. This problem has been numerically explored by Ribando and Torrance [12]. A representative set of results in Ref. [12] for a heat-flux-based Rayleigh number (equivalent to Ra Q_w in this paper) of 200 and an aspect ratio of 1.67 is chosen for comparison. Ribando and Torrance [12] used a 16×16 grid and the upwind scheme for the convective term in the energy equation. Therefore, to be comparable, calculations are carried out using a relatively coarse 22×22 grid as well as the upwind scheme. The present prediction for the maximum value of the stream function, $\Psi_{max} = 3.237$, agrees with the value of 3.21 reported by Ribando and Torrance [12]. Moreover, the temperature fields (not shown here) are also indistinguishable. Finally, it is of interest to point out that the same calculation but employing the power law instead of the upwind scheme results in $\Psi_{max} = 3.35$.

To validate the present algorithm for the case of two-phase flow, another example is considered where the single-phase region is conduction controlled and the two-phase region is dominated by one-dimensional countercurrent two-phase percolation. This situation typically occurs in low-permeability media, and an appropriate model is formulated in the appendix. The liquid saturation profile obtained from the model is compared with that from the numerical simulation using the present algorithm, as shown in Figure 2. It can be seen that the 12- and 22-grid lines lead to fairly close agreement with the semi-analytical predictions, which are obtained via the fourth-order Runge-Kutta method. The 42-grid lines produce an excellent match.

RESULTS AND DISCUSSION

As noted above, the problem under investigation is governed by a large number of dimensionless parameters. Instead of covering wide ranges of all of these parameters, results are obtained only for a water-steam–glass bead system at
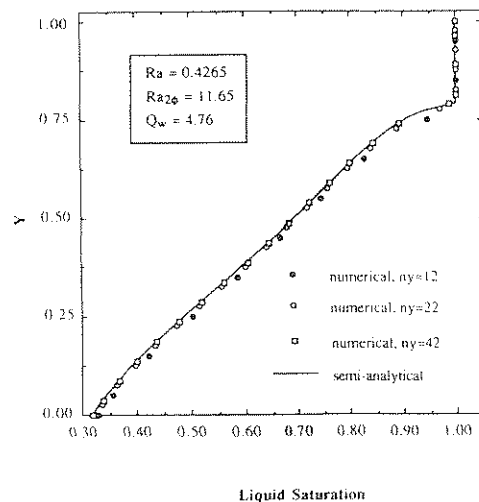

Figure 2. Comparison of liquid saturation profiles predicted numerically by the complete two-dimensional model and semi-analytically by the one-dimensional model presented in the appendix.

atmospheric pressure, with the temperature difference and layer thickness fixed (i.e., $T_{sat} = 373$ K, $T_o = 293$ K, and $L_h = 0.2$ m). Attention is focused on the effects of the Rayleigh number (either $Ra_{2\phi}$ or Ra), the dimensionless bottom heat flux (Q_w), and the geometric aspect ratio (A). To vary $Ra_{2\phi}$ or Ra while keeping Q_w and A constant implies a variation in the permeability of the porous layer. Similarly, a variation in Q_w is practically achieved by adjusting the bottom heat flux, and a change in A is realized by changing the width of the porous bed. Comparisons are first made to previous studies available in the literature, which include three independent sets of experiments of two-phase flow in porous media of various permeabilities [13–16] as well as the linear stability results reported in Ref. [10]. This is followed by a parametric study. Thermophysical properties used for the water-steam–glass bead system are listed in Table 1. All numerical simulations carried out in this study are summarized in Table 2. In the table there appears a new quantity, ε_v, which is the volume fraction of the vapor phase present in the entire porous bed, i.e.,

$$\varepsilon_v = A \int_0^{1/A} \int_0^1 (1 - s) \, dX \, dY \tag{38}$$

The vapor fraction is a direct measure of the boiling strength and the extent of the resulting two-phase zone. From an experimental point of view, the vapor volume fraction is a convenient quantity to measure, since the liquid displacement due to boiling is just equal to $\varepsilon_v(\rho_l - \rho_v)$.

Comparisons with Previous Studies

The three independent sets of experiments listed in Table 2 correspond to low-, intermediate-, and high-permeability porous media [13–16]. The present numerical simulations are designed to explain the experimental observations made in these studies [13–16].

In low-permeability media ($K \approx 10^{-11}$ m^2), Bau and Torrance's experimental data [13] indicate that the liquid region is conductive before and after the onset of boiling. This is now verified by the present numerical simulations, as shown in the first two cases of Table 2. No thermal convection is found without boiling simply

Table 1. Thermophysical Property Data for a Water-Steam–Glass Bead System

Property	Symbol	Value	Liquid	Vapor	Unit
Density	ρ		957.9	0.598	kg/m^3
Specific heat	c		4.178×10^3	1.548×10^3	J/kg K
Kinetic viscosity	ν		4.67×10^{-7}	2.012×10^{-5}	m^2/s
Expansion coefficient	β		5.23×10^{-4}	–	K^{-1}
Thermal conductivity	k_{eff}		0.85	–	W/m K
Surface tension	σ		0.0588	–	N/m
Heat capacitance ratio	$\rho_s c_s/\rho_l c_l$	0.5820			–
Latent heat	h_{fg}	2.257×10^6			J/kg
Porosity	ε	0.35			

Table 2. Summary of the Numerical Simulations Performed

Case	$Ra_{2\phi}$	(Ra)	A	Q_w	Convection	Boiling	Vapor volume fraction, $\varepsilon_v \times 10^3$	Features
1	200	(8.5)	1	1.0	no	no	–	$K = 10^{-11}$ m^2; conduction before and after boiling;
2	200	(8.5)	1	2.0	no	yes	20.3	Bau and Torrance's experiments [13]
3	1400	(60)	1	1.0	no	no	–	$K = 7 \times 10^{-11}$ m^2; conduction before boiling and
4	1400	(60)	1	2.5	yes	yes	1.03	convection after boiling;
5	1400	(60)	1	3.0	yes	yes	1.71	Sondergeld and Turcotte's
6	1400	(60)	1	4.0	yes	yes	3.56	experiments [14, 15]
7	1400	(60)	0.5	4.0	yes	yes	0.92	
8	2000	(85)	1	2.0	yes	no	–	$K = 10^{-10}$ m^2; convection before and after boiling;
9	2000	(85)	1	5.0	yes	yes	0.96	transition to a conductive liquid
10	2000	(85)	1	10.0	yes	yes	6.71	layer at high heat fluxes; Bau and
11	2000	(85)	1	15.0	no	yes	41.1	Torrance's experiments [16]
12	617	(25)	1	2.0	yes	yes	2.4	$K = 3 \times 10^{-11}$ m^2; unicellular convection

because Ra is smaller than the critical value as obtained from a linear stability analysis. Even in the presence of boiling (case 2), the phase interface between the single- and two-phase regions remains horizontal, as can be seen from the dashed line in Figure 3. The isotherms in the overlying liquid region and the isoliquid saturation lines in the underlying two-phase region in Figure 3 suggest that the
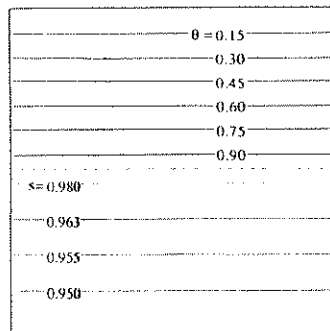

Figure 3. Steady state temperature and liquid saturation fields for case 2 (Ra = 8.5, $Q_w = 2.0$, and $A = 1$). The dashed line denotes the phase interface between the liquid and the two-phase regions.

transport phenomena in such a low-permeability medium are characterized by pure heat conduction in the liquid region and one-dimensional vertical countercurrent percolation of liquid and vapor in the two-phase zone. Isotherms depicted in the present paper represent lines of constant $\theta = (T - T_0)/(T_{sat} - T_0)$, with the top boundary and the phase interface represented by $\theta = 0$ and 1, respectively. The isoliquid saturation lines, however, denote absolute values. The temperature distribution in the liquid region is horizontally uniform and linear along height, as it should be. In contrast, the liquid saturation profile exhibits a nonlinear variation with height. This is because the transport properties in the two-phase region vary strongly with the liquid saturation.

In porous media of intermediate permeabilities, the picture of boiling is substantially different from what is described above. As observed by Sondergeld and Turcotte [14], thermal convection does not occur in the absence of boiling, but starts with the onset of boiling. Furthermore, a visualization study by the same authors [15] revealed distinct cellular convection patterns that involve both the overlying liquid layer and the underlying two-phase zone. Their experimental runs are now numerically simulated, and Figures 4–6 illustrate the predicted isotherm, isoliquid saturation, streamline, and phase velocity distributions for dimensionless bottom heat fluxes of $Q_w = 1.0$, 2.5, and 4.0 (cases 3, 4, and 6 in Table 2, respectively). The streamlines are based on the dimensionless mixture velocity (which is the liquid velocity in the liquid region), and the liquid and vapor velocity vector plots correspond to $\mathbf{u}_l$ and $\bar{\rho}\mathbf{u}_v$, respectively.

All three cases have the value Ra = 60, which corresponds to $K = 7.0 \times 10^{-11}$ m², as in Sondergeld and Turcotte's experiments [14, 15]. The first numerical run is performed for $Q_w = 1.0$ (case 3), and the predicted temperature profile shown in Figure 4 indicates no evidence of thermal convection. It is worth mentioning that, in the pure conduction case, $Q_w = 1.0$ marks the onset of boiling because the reference flux used in the definition of Q_w, $k_{eff}(T_{sat} - T_0)/H$, represents the maximum conductive flux across a liquid-saturated layer.

When Q_w increases to 2.5 (case 4), boiling initiates at the bottom surface, as shown in Figure 5a. It is more important to notice that thermal convection is triggered immediately upon the onset of boiling. The cellular convection is so strong that the phase interface is highly distorted. Figure 5b further illustrates that there are two convective cells present in the liquid region and the streamlines penetrate into the two-phase zone. Figures 5c and 5d depict the phase velocity
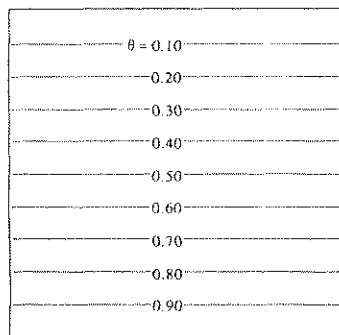

Figure 4. Steady state temperature field for case 3 (Ra = 60, Q_w = 1, and A = 1). This case is marginal to the onset of boiling.
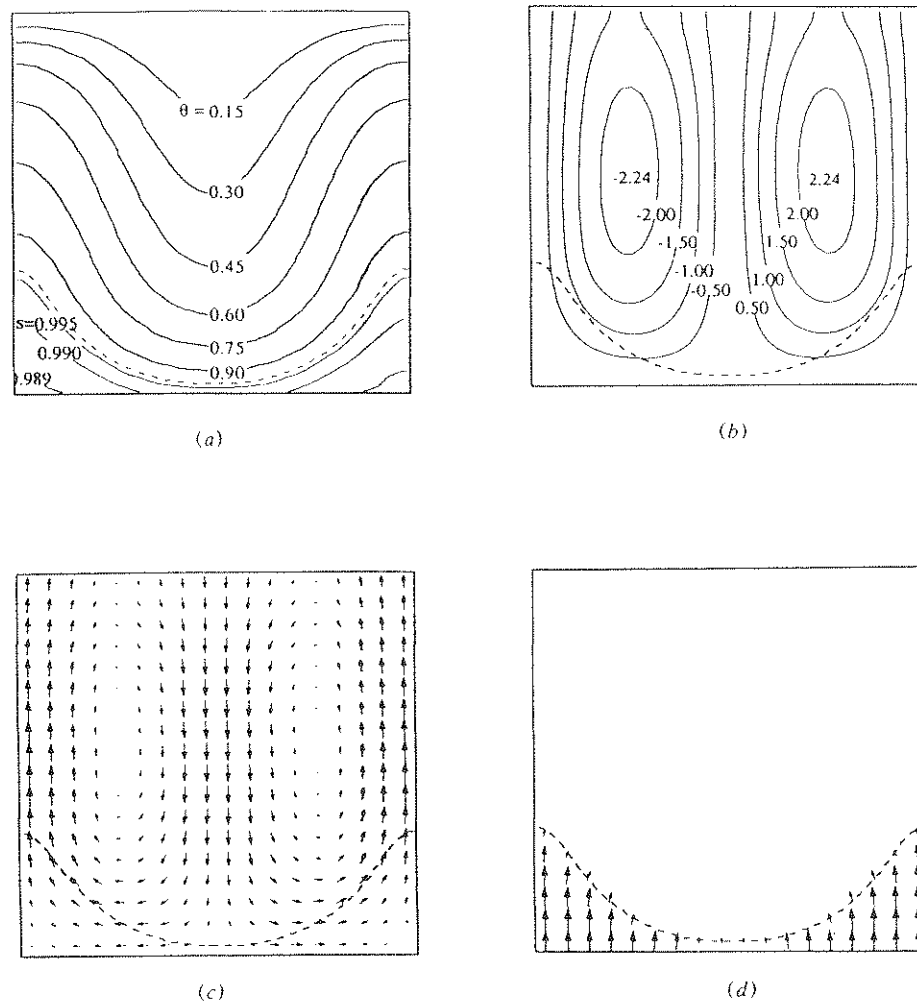
Figure 5. Steady state solution for case 4 (Ra = 60, Q_w = 2.5, and A = 1): (a) isotherms and isoliquid saturation lines, (b) streamlines for the two-phase mixture, (c) liquid velocity vectors ($|\mathbf{u}_l|_{max} = 0.15 \times 10^{-4}$ m/s), and (d) vapor velocity vectors ($|\tilde{\rho}\mathbf{u}_v|_{max} = 0.38 \times 10^{-6}$ m/s).

fields. It is clear that the vapor flows primarily vertically upward, whereas the liquid phase has considerable lateral motion. The simulation results for this case agree excellently with the experimental observations made by Sondergeld and Turcotte [14, 15]. When the bottom heat flux increases further, the underlying two-phase zone expands, and thermal convection is more evident, as shown in Figures 6a–6d (case 6). The fact that the formation of a two-phase zone can drive thermal convection can be understood by recalling that the two-phase Rayleigh number, $Ra_{2\phi}$, is substantially higher than the critical single-phase Rayleigh number, Ra. Although the present steady state investigation provides results that are consistent with the experiments, the detailed mechanisms through which natural convection is
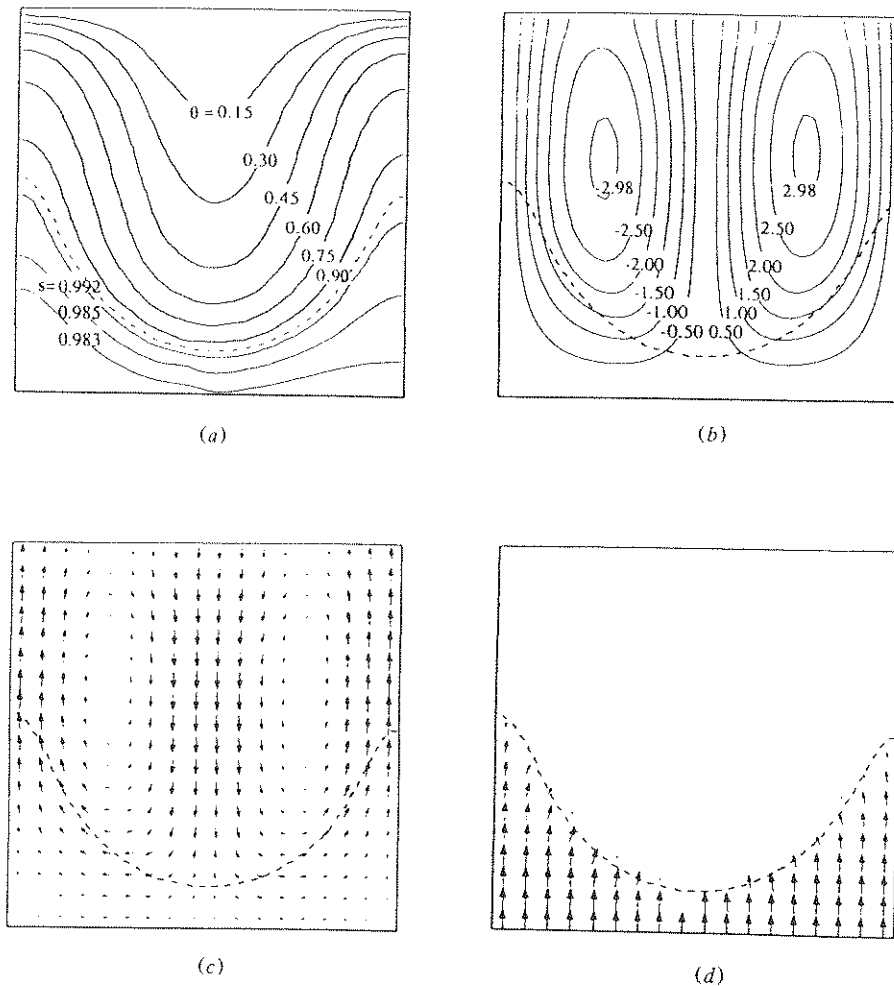
Figure 6. Steady state solution for case 6 (Ra = 60, Q_w = 4.0, and A = 1): (*a*) isotherms and isoliquid saturation lines, (*b*) streamlines for the two-phase mixture, (*c*) liquid velocity vectors ($|u_l|_{max}$ = 0.21 × 10^{-4} m/s), and (*d*) vapor velocity vectors ($|\bar{\rho}u_v|_{max}$ = 0.63 × 10^{-6} m/s).

induced by boiling have not been identified. For this purpose, a transient simulation would be helpful because it can reveal the evolution of boiling and the interactions between the single- and two-phase regions.

The last simulation set (cases 8–11) for a relatively high permeability (K = 10^{-10} m²) is conducted for comparison with Bau and Torrance's experiments [16]. In these cases, the Rayleigh number (Ra = 85) is larger than the critical value for the onset of single-phase natural convection, so that steady cellular convection prevails before the onset of boiling. This is shown by the temperature and streamline contours depicted in Figures 7a and 7b for Q_w = 2.0 (case 8). The dashed line appearing on the very left and right corners suggests that this case is

marginal to the onset of boiling. When Q_w is raised to 5.0 (case 9), a two-phase region develops at the bottom, and thermal convection persists (see Figure 8). Again, it is seen that the streamlines penetrate into the two-phase region, implying that there exists a strong interaction between the boiling and natural convection flows in the two regions. The phase velocity vector plots exhibit similar features as in Figures 5 and 6. When Q_w is further increased (case 10), the two-phase zone occupies almost half of the porous bed, and the interaction between boiling and natural convection is more pronounced (see Figure 9). However, when Q_w is finally raised to 15.0 (case 11), thermal convection in the liquid region disappears, and the phase interface becomes horizontally flat, as shown in Figure 10. The high heat flux is, instead, achieved by conduction through the thin liquid layer.

To summarize, the present results for high-permeability porous media show that the liquid layer is convective before the onset of boiling and stays convective after boiling, which is consistent with the experiments conducted in Ref. [16]. Furthermore, Bau and Torrance [16] observed that, at large bottom heat fluxes (e.g., $q_w = 7 \text{ kW/m}^2$ in their experiments) the overlying liquid region reverts back to a conductive heat transfer mode, which is again in agreement with the present simulations. For even higher heat fluxes (e.g., $q_w = 11 \text{ kW/m}^2$), Bau and Torrance's experiments [16] indicated that the system is oscillatory in time, and thus the present steady state analysis is expected to become invalid.

In addition to the above qualitative comparisons, more quantitative comparisons are attempted below. The experiments of Sondergeld and Turcotte [14] are best suited because the properties of the porous medium tested are less uncertain and the experimental conditions are well defined. Figure 11 compares the measured and predicted volume fractions of the vapor phase present in the porous layer for different bottom heat fluxes. The solid line in Figure 10 represents the present numerical results, and the dashed line corresponds to the semi-analytical solution of the one-dimensional model presented in the appendix, which is applica-
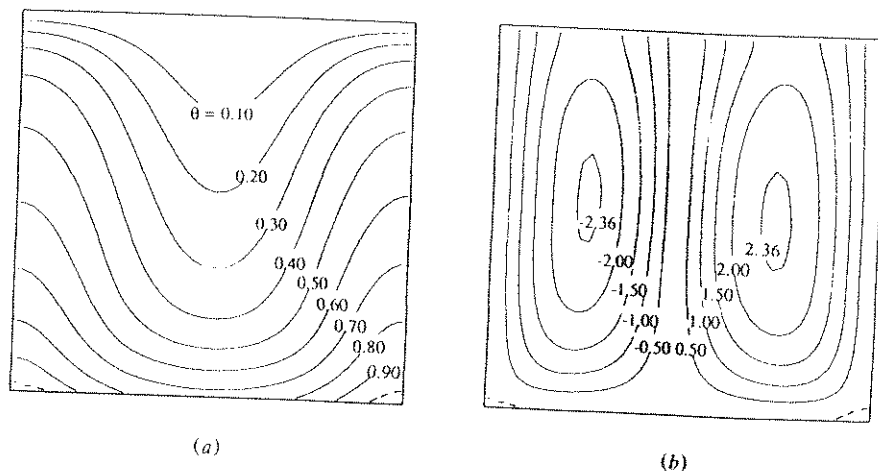

(a)   (b)

Figure 7. Steady state solution for case 8 (Ra = 85, Q_w = 2.0, and A = 1): (a) isotherms and (b) streamlines.
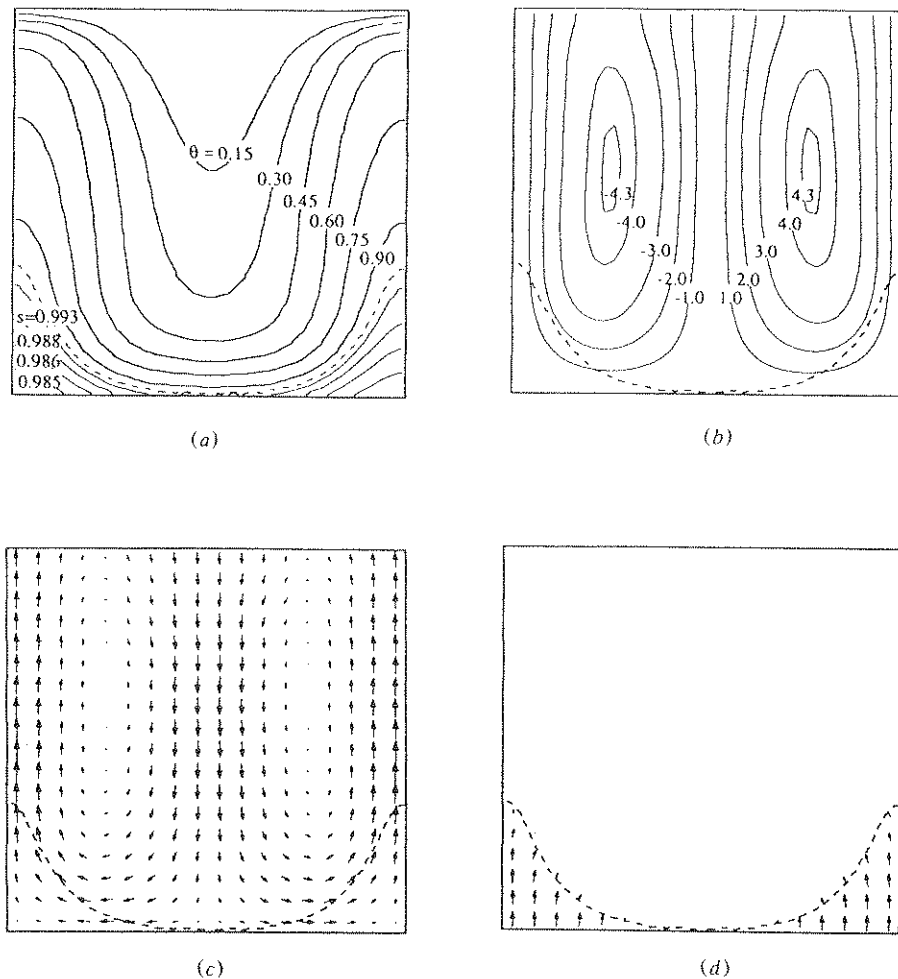
Figure 8. Steady state solution for case 9 (Ra = 85, Q_w = 5.0, and A = 1): (a) isotherms and isoliquid saturation lines, (b) streamlines for the two-phase mixture, (c) liquid velocity vectors ($|u_l|_{max}$ = 0.31 × 10^{-4} m/s), and (d) vapor velocity vectors ($|\tilde{\rho} u_v|_{max}$ = 1.05 × 10^{-6} m/s).

ble to cases where the overlying liquid layer is conduction controlled and the two-phase region is dominated by one-dimensional two-phase countercurrent percolation. The squares represent the data points measured in Ref. [14]. It can be seen that at low and intermediate bottom heat fluxes the two-dimensional numerical model predicts the experimental data reasonably well, while the one-dimensional analytical model leads to considerable overpredictions. Beyond a certain value of the bottom heat flux, the two-dimensional results merge into the one-dimensional solution line. This is because, at high heat fluxes, the liquid region shrinks and reverts back to the conduction regime, and the flow inside the two-phase zone becomes one-dimensional, as discussed earlier. However, the

experimental data for ε_v do not follow this trend, but instead approach an upper limit at high heat fluxes [14]. This deviation between theory and experiment is suspected to be caused by fluidization of the solid matrix under violent boiling, which creates additional void spaces through which the vapor can pass. As mentioned above, the experiments performed by Bau and Torrance [16] do confirm the transition of the flow from a two- to a one-dimensional mode at high fluxes. More experiments are needed to resolve the issue.

Recalling that the present two-phase mixture model is mathematically exactly equivalent to the separate flow model, the present numerical results can be used to
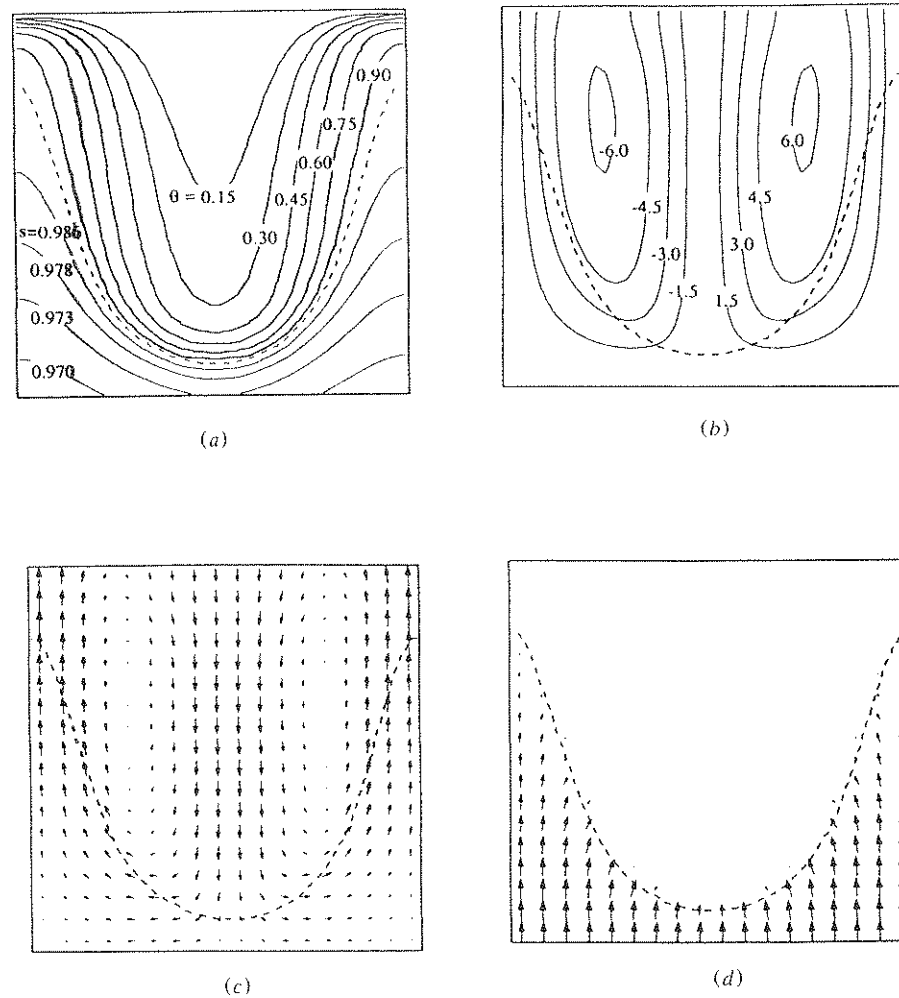

(a)

(b)

(c)

(d)

Figure 9. Steady state solution for case 10 (Ra $= 85$, $Q_w = 10.0$, and $A = 1$): (a) isotherms and isoliquid saturation lines, (b) streamlines for the two-phase mixture, (c) liquid velocity vectors ($|\mathbf{u}_l|_{max} = 0.43 \times 10^{-4}$ m/s), and (d) vapor velocity vectors ($|\tilde{\rho}\mathbf{u}_v|_{max} = 1.57 \times 10^{-6}$ m/s).
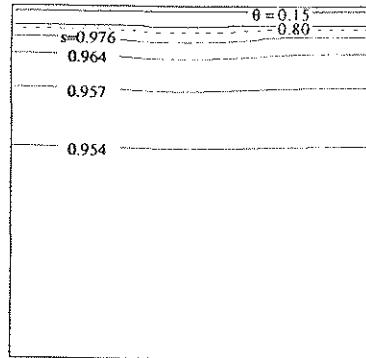
Figure 10. Steady state temperature and liquid saturation fields for case 11 (Ra = 85, Q_w = 15.0, and A = 1).

verify the linear stability results of Ramesh and Torrance [10] based on the latter approach. Figure 7 shows that in a porous layer with Ra ≈ 85, the onset of boiling takes place at a dimensionless bottom heat flux Q_w of approximately 2.0. This finding validates the boiling onset curve labeled "BE" in the stability map developed by Ramesh and Torrance [10]. In addition, Table 2 indicates that for Ra ≈ 85, the transition from a convective to a conductive overlying liquid layer occurs at a heat flux between 10 and 15. However, the convection onset curve labeled "BD" in the same map [10] indicates Q_w ≈ 7.5 for the transition. This quantitative discrepancy has recently been found to be related to a hysteresis effect present in the system under consideration. By performing a transient analysis [17], it has been shown that the transition from a convective to a conductive overlying liquid layer can occur over a wide range of bottom heat fluxes, i.e., $8.9 \leq Q_w \leq 17.5$, depending on how the heat flux is changed (i.e., decreasing or increasing). The slight difference between the linear stability result and the minimum heat flux (i.e., Q_w = 8.9) for the transition as found in the transient numerical simulations is possibly due to the fact that the present numerical analysis includes the capillary effect, which was neglected in the linear stability analysis.
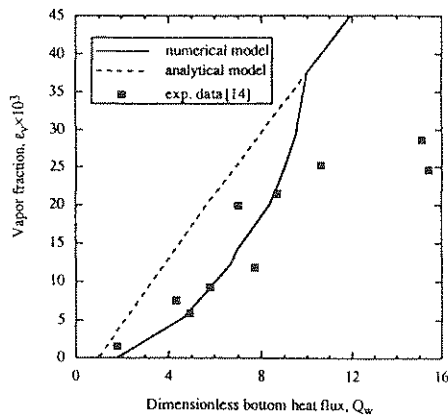

Figure 11. Comparison of the measured and predicted vapor volume fractions as a function of the dimensionless bottom heat flux Q_w for L_h = 0.1984 m and $K = 7 \times 10^{-11}$ m².

Parametric Study

In this subsection the effects are investigated of three major parameters that characterize the present system, namely, the Rayleigh number, $Ra_{2\phi}$ or Ra, the dimensionless bottom heat flux Q_w and the geometric aspect ratio A.

The effect of the Rayleigh number can be understood by inspecting the cases with the same heating strength (say, $Q_w = 2.0$) and Ra = 8.5, 25, and 85. At a low Rayleigh number (Ra = 8.5, case 2), the energy input at the bottom is dissipated purely by conduction through the liquid region; thereby, a large two-phase zone forms. As Ra increases (Ra = 25, case 12), unicellular natural convection is induced by boiling, and the heat is more effectively transferred to the top boundary, so that the range of the two-phase zone is reduced. This is shown in Figures 12a and 12b. When Ra finally increases to 85 (case 8), thermal convection in the liquid region is so strong that the two-phase region completely vanishes.

The effect of Q_w has been discussed earlier when comparing Figures 4–6.

The next parameter of interest is the aspect ratio of the domain, A. The effect of this parameter is illustrated by comparing Figure 6 ($A = 1.0$, case 6) and Figure 13 ($A = 0.5$, case 7). The values of the other dimensionless groups in these figures are identical (i.e., Ra = 60 and $Q_w = 4.0$). The case with $A = 0.5$ is calculated using a 42×82 grid. It is interesting to note that the flow inside the rectangular domain intensifies and the two-phase zone is accordingly reduced in size.

In closing, it should be pointed out that the CPU time for a typical run possessing strong multidimensional effects and using the 42×42 grid is about 40 s on a DN10,000 workstation.

CONCLUSIONS

A numerical application of the newly developed two-phase mixture model [5] has been provided for boiling with natural convection in a horizontal porous layer heated from below. A fixed grid solution methodology has been developed based on the new model, and a flexible and convenient means of solving complex coupled single- and two-phase flows with phase change in capillary porous media has been established within the framework of the well-established control-volume-based finite difference scheme. Unlike previous numerical procedures, the present one eliminates the need to explicitly track moving interfaces that are internal to the domain and to prescribe complex compatibility conditions at these interfaces. It is also shown that the complex problem under consideration can be reduced to a level of computational effort generally associated with the solution of strongly coupled and nonlinear single-phase problems.

The numerical results have been compared with a number of experimental investigations, and good agreement is achieved. Four different flow patterns that have previously been observed in experiments have been successfully predicted. They are (1) conductive liquid layer before and after the onset of boiling, (2) conductive liquid layer before the onset of boiling but convective liquid layer after the onset of boiling, (3) convective liquid layer before and after the onset of
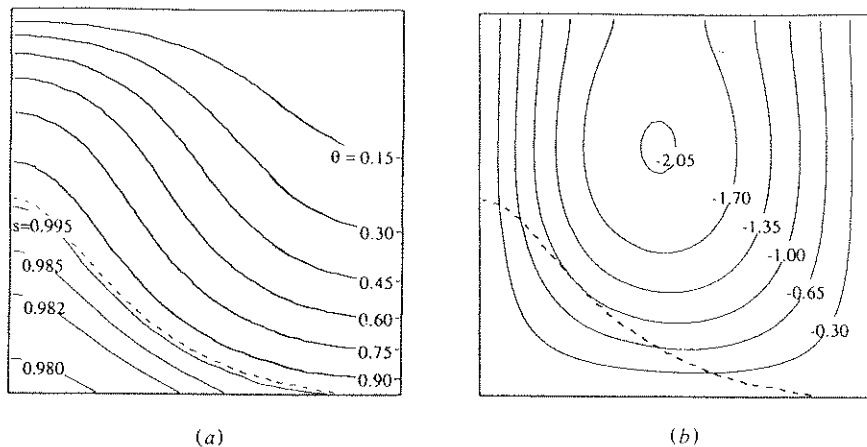
Figure 12. Steady state solution for case 12 (Ra = 25, Q_w = 2.0, and A = 1): (a) isotherms and isoliquid saturation lines and (b) streamlines.

boiling, and (4) convective liquid layer at low heat fluxes but conductive liquid layer at high heat fluxes in the presence of boiling. The numerical results also illustrate the effects of major parameters such as Rayleigh number, dimensionless bottom heat flux, and aspect ratio.

## APPENDIX: ANALYTICAL MODEL FOR STEADY ONE-DIMENSIONAL PROBLEMS

Under steady state conditions, the mixture velocity vanishes, as is evident from the continuity equation. Thus the energy equation, Eq. (10), valid in both the single- and two-phase regions, reduces to

$$\nabla \cdot \left(\frac{\Gamma_h}{\rho} \nabla H \right) + \nabla \cdot \left[f(s) \frac{K \Delta \rho h_{fg}}{\nu_v} \mathbf{g} \right] = 0 \qquad \text{(A1)}$$
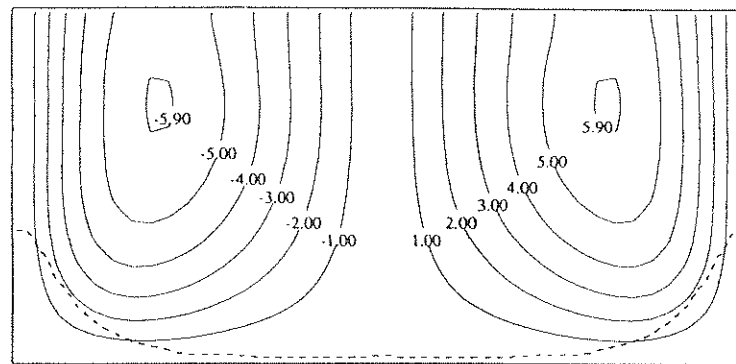
Liquid Region

In the liquid region, the second term in Eq. (A1) drops out, and the one-dimensional heat conduction equation is recovered, which gives the following linear temperature profile:

$$\theta = \frac{T - T_o}{T_{sat} - T_o} = \frac{1 - Y}{1 - 1/Q_w} \qquad \text{(A2)}$$
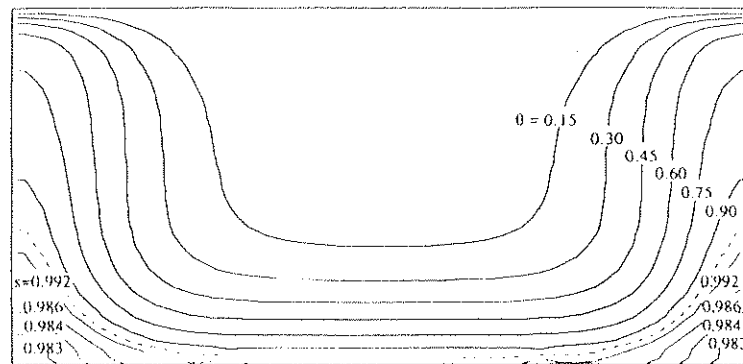
(a)

(b)

Figure 13. Steady state solution for case 7 (Ra = 60, Q_w = 4.0, and A = 0.5):
(a) isotherms and isoliquid saturation lines and (b) streamlines.

where Y is the dimensionless coordinate in the vertical direction and the phase change interface is located at $Y = 1/Q_w$. Obviously, for a two-phase region to exist, the dimensionless heat flux Q_w must be greater than unity.

Two-Phase Region

Integrating Eq. (A1) once and rewriting the resultant equation in terms of the liquid saturation yields the following dimensionless first-order differential equation for the liquid saturation:

$$\mathrm{Le}_c \left(-\frac{dJ(s)}{ds} \right) \frac{ds}{dY} + (1 - \bar{\rho})\, \mathrm{Ra}_{2\phi} = \frac{Q_w}{\lambda} \left(\frac{1}{k_{ri}} + \frac{\bar{\nu}}{k_{rv}} \right) \tag{A3}$$

Its corresponding boundary condition is, at $Y = 1 - 1/Q_w$ (phase-change interface),

$$s = 1.0 \qquad\qquad (A4)$$

The liquid saturation profile along the height can therefore be obtained by solving Eq. (A3) subject to Eq. (A4), using the standard fourth-order Runge-Kutta method.

REFERENCES

1. J. Bear, *Dynamics of Fluids in Porous Media*, Elsevier, New York, 1978.
2. M. B. Allen III, Numerical Modeling of Multiphase Flow in Porous Media, *Adv. Water Resour.*, vol. 8, pp. 162–187, 1985.
3. P. S. Ramesh and K. E. Torrance, Numerical Algorithm for Problems Involving Boiling and Natural Convection in Porous Materials, *Numer. Heat Transfer Part B*, vol. 17, pp. 1–24, 1990.
4. M. Chung and I. Catton, Post-Dryout Heat Transfer in a Multi-Dimensional Porous Bed, *Nucl. Eng. Des.*, vol. 128, pp. 289–304, 1991.
5. C. Y. Wang and C. Beckermann, A Two-Phase Mixture Model of Liquid-Gas Flow and Heat Transfer in Capillary Porous Media, Part I: Formulation, *Int. J. Heat Mass Transfer*, vol. 36, pp. 2747–2758, 1992.
6. C. Y. Wang and C. Beckermann, A Two-Phase Mixture Model of Liquid-Gas and Heat Transfer in Capillary Porous Media, Part II: Application to Pressure-Driven Boiling Flow Adjacent to a Vertical Heated Plate, *Int. J. Heat Mass Transfer*, vol. 36, pp. 2759–2768, 1992.
7. P. J. Roache, *Computational Fluid Dynamics*, Hermosa, Albuquerque, New Mexico, 1976.
8. S. Patankar, *Numerical Heat Transfer and Fluid Flow*, Hemisphere, Washington, D.C., 1980.
9. K. S. Udell, Heat Transfer in Porous Media Heated from Above with Evaporation, Condensation, and Capillary Effects, *ASME J. Heat Transfer*, vol. 105, pp. 485–492, 1983.
10. P. S. Ramesh and K. E. Torrance, Stability of Boiling in Porous Media, *Int. J. Heat Mass Transfer*, vol. 33, pp. 1895–1908, 1990.
11. V. X. Tung and V. K. Dhir, Finite Element Solution of Multi-Dimensional Two-Phase Flow through Porous Media with Arbitrary Heating Conditions, *Int. J. Multiphase Flow*, vol. 16, pp. 985–1002, 1990.
12. R. J. Ribando and K. E. Torrance, Natural Convection in a Porous Medium: Effects of Confinement, Variable Permeability, and Thermal Boundary Conditions, *ASME J. Heat Transfer*, vol. 98, pp. 42–48, 1976.
13. H. H. Bau and K. E. Torrance, Boiling in Low-Permeability Porous Media, *Int. J. Heat Mass Transfer*, vol. 25, pp. 45–55, 1982.
14. C. H. Sondergeld and D. L. Turcotte, An Experimental Study of Two-Phase Convection in a Porous Medium with Applications to Geological Problems, *J. Geophys. Res.*, vol. 82, pp. 2045–2053, 1977.
15. C. H. Sondergeld and D. L. Turcotte, Flow Visualization Studies of Two-Phase Thermal Convection in a Porous Layer, *Pure Appl. Geophys.*, vol. 117, pp. 321–330, 1978.
16. H. H. Bau and K. E. Torrance, Thermal Convection and Boiling in a Porous Medium, *Lett. Heat Mass Transfer*, vol. 9, pp. 431–441, 1982.
17. C. Y. Wang, C. Beckermann, and C. Fan, Transient Natural Convection and Boiling in a Porous Layer Heated from Below, presented at 10th International Heat Transfer Conference, Brighton, UK, 1994.